Waveguide or Not? Revised Ground-Motion Simulations for Greater Los Angeles from the M 7.8 ShakeOut Earthquake Scenario

Te-Yang Yeh[*1] and Kim B. Olsen[1]

Abstract

The ShakeOut scenario of an M 7.8 northwestward rupture on the southern San Andreas fault (SSAF) (Jones *et al.*, 2008) predicted significant long-period ground-motion amplification in the greater Los Angeles, California, area, caused by a waveguide from interconnected sedimentary basins. However, the early ShakeOut ground-motion simulations omitted important model features with immature versions of the velocity structure and fault geometry. Here, we present 0–1 Hz 3D numerical wave propagation simulations for the ShakeOut scenario including surface topography, as well as updated high-resolution velocity structures and SSAF geometry. Spectral accelerations at 3 s are increased by the local high-resolution basin models (25%–45%) but decreased from complexity in velocity and density updates outside the basins (65%–100%) and inclusion of surface topography (~30%). The updated model reduces the simulated long-period ground motions in the waveguide by 60%–70%, bringing the predictions significantly closer to the values by a leading Next Generation Attenuation-West2 ground-motion model.

Cite this article as Yeh, T.-Y., and K. B. Olsen (2024). Waveguide or Not? Revised Ground-Motion Simulations for Greater Los Angeles from the **M** 7.8 ShakeOut Earthquake Scenario, *Seismol. Res. Lett.* **XX**, 1–12, doi: 10.1785/0220240242.

Supplemental Material

Introduction

The seismic hazards anticipated for a large seismic event along the southern segment of the San Andreas fault (SSAF) (Field, 2008) inspired the multi-institutional Great Southern California **M** 7.8 ShakeOut scenario (Jones *et al.*, 2008). The primary objective of the ShakeOut scenario was to promote awareness and preparedness for an impending major seismic event in the densely populated southern California region (Jones and Benthien, 2011; Porter *et al.*, 2011). As documented in Jones *et al.* (2008), the ShakeOut scenario used a kinematic rupture model based on the best available geological and geophysical information at the time, the 3D fault geometry from the Statewide California Earthquake Center (SCEC) Community Fault Model (CFM, Plesch *et al.*, 2007), as well as the estimated rupture extent and slip distribution from paleoseismic constraints (see Text S1, available in the supplemental material to this article). Physics-based 3D numerical simulations were then used to estimate the expected ground motions in southern California (see domain in Fig. 1) up to 1 Hz (Bielak *et al.*, 2010), or up to 10 Hz using a hybrid stochastic method (Graves *et al.*, 2008, 2011; Jones *et al.*, 2008).

Ground-motion simulations of the ShakeOut scenario revealed a strong waveguide effect from the San Gabriel basin to the Los Angeles basin because amplified surface waves travel through the interconnected basins. Day *et al.* (2012) used an adjoint procedure and showed that the waveguide excitation is greatest for slip concentrated between the northern Coachella valley and the Transverse Ranges, propagating to the northeast and with rupture velocities between 3250 and 3500 m/s. The predicted ground motions from the ShakeOut scenario, generating long-period peak ground velocities (PGVs) as large as 250 cm/s along the waveguide, have been used for evaluation of seismic risks in the greater Los Angeles areas (Krishnan and Muto, 2008; Taciroglu and Khalili-Tehrani, 2008; Lynch *et al.*, 2011; Porter *et al.*, 2011).

The early ShakeOut numerical studies described earlier (Graves *et al.*, 2008, 2011; Olsen *et al.*, 2009; Bielak *et al.*, 2010) including a more recent study using a more accurate fault geometry by Fuis *et al.* (2017), adopted the SCEC Community Velocity Model (CVM) version CVM-S4 (abbreviated CVMS hereafter). CVMS is based on the combination of travel-time tomography and structural and geotechnical

1. Department of Earth and Environmental Sciences, San Diego State University, San Diego, California, U.S.A., https://orcid.org/0000-0002-9146-6804 (T-YY); https://orcid.org/0000-0002-3078-485X (KBO)

*Corresponding author: tyeh2@sdsu.edu

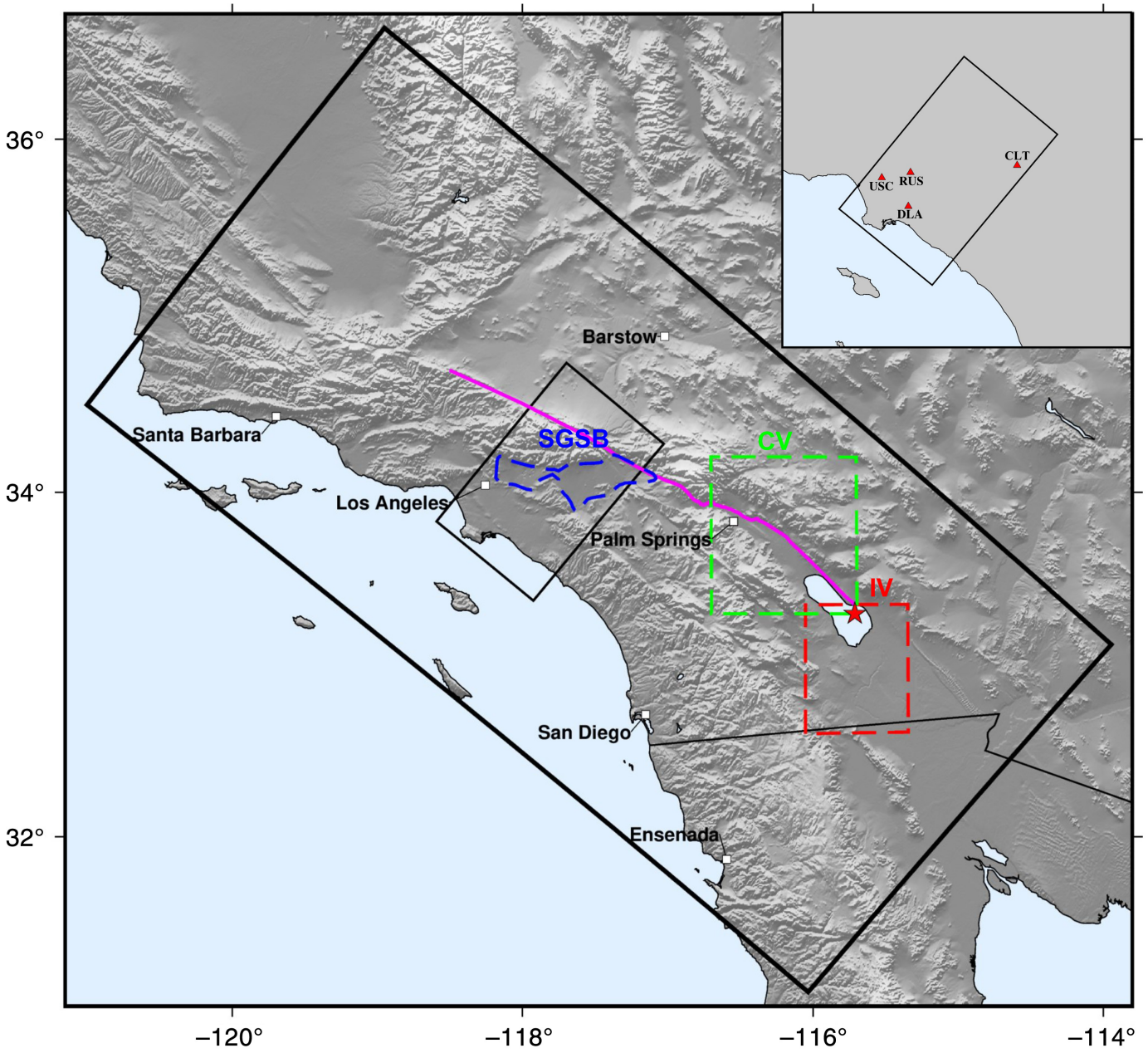

description of major basins in southern California (Magistrale *et al.*, 2000; Kohler *et al.*, 2003). However, since these studies, major updates of CVMS have been obtained with full-waveform tomography (Lee *et al.*, 2014), resulting in CVM-S4.26.M01 (abbreviated to CVMSI from here on), greatly enhancing the resolution of the crustal structure outside the major basins in southern California. In addition, high-resolution models covering the sedimentary basins along the waveguide (San Gabriel basin–Chino basin–San Bernardino basin) as well as the regions closest to the ShakeOut rupture source (Imperial valley and Coachella valley) have been obtained from ambient noise tomography (Li *et al.*, 2023) and seismic imaging from active and earthquake sources (Persaud *et al.*, 2016; Ajala *et al.*, 2019). Finally, we note that the earlier ShakeOut simulations employed a flat-free surface boundary condition,

Figure 1. Location map with the large black rectangle depicting the ShakeOut simulation domain and the small black rectangular area used for comparison of predicted ground motions in the major basins where the waveguide effect occurs. The dashed polygons depict the domains of local high-resolution models (CV, Coachella valley model by Ajala *et al.*, 2019; IV, Imperial valley model by Persaud *et al.*, 2016; SGSB, San Gabriel–Chino–San Bernardino basins model by Li *et al.*, 2023), and the magenta line shows the surface projection of the southern San Andreas fault (SSAF) that ruptured in the ShakeOut scenario from Jones *et al.* (2008). The inset map depicts the domain for comparison of ground motions and the locations of stations for waveform comparison. The color version of this figure is available only in the electronic edition.

TABLE 1
List of Models Used in This Study

Model No.	Base Model	Surface Topography	Local Models Included	LVT	Fault Geometry	SSH
1	CVMS	No	No	No	CFM	No
2	CVMSI	No	No	No	CFM	No
3	CVMSI	Yes	No	No	CFM	No
4	CVMSI	Yes	IV + CV	No	CFM	No
5	CVMSI	Yes	IV + CV + SGSB	No	CFM	No
6	CVMSI	Yes	IV + CV + SGSB	Yes (z_T = 700 m)	CFM	No
7	CVMSI	Yes	IV + CV + SGSB	Yes (z_T = 700 m)	Fuis *et al.* (2017)	No
8*	CVMSI	Yes	IV + CV + SGSB	Yes (z_T = 700 m)	Fuis *et al.* (2017)	σ = 7.5%, L_x = 8 km, H = 0.15

CFM, Community Fault Model; CV, Coachella valley model by Ajala *et al.* (2019); CVMS, Community Velocity Model version S4; CVMSI, Community Velocity Model-S4.26.M01; IV, Imperial valley model by Persaud *et al.* (2016); LVT, low-velocity taper; SGSB, San Gabriel–Chino–San Bernardino basin model by Li *et al.* (2023); SSH, statistical distribution of velocity and density heterogeneities.
*Five realizations were generated for models with statistical models of heterogeneities.

thereby excluding the effects of surface topography, which has been shown to be important for accurately predicting ground motion in southern California (e.g., Ajala *et al.*, 2022; Hu *et al.*, 2022a).

The primary objective of this article is to investigate the effects of updated or excluded model features on the resulting long-period ground motions derived from a series of 0–1 Hz numerical simulations conducted for the ShakeOut scenario (Jones *et al.*, 2008), starting from the velocity and source models adopted in the early ShakeOut studies (Graves *et al.*, 2008; Jones *et al.*, 2008; Olsen *et al.*, 2009; Bielak *et al.*, 2010). In addition, we explore potential sources of uncertainties of the predicted ground motions within our results, leading to the estimate of the most up-to-date predictions for ground motions in the greater Los Angeles area for the ShakeOut scenario, with emphasis on the presence and severity of waveguide amplification of long-period ground motion in greater Los Angeles.

Numerical Method and Velocity Models

To quantify the effects of the different model features contributing to the ground motions from the ShakeOut scenario, we performed 0–1 Hz 3D viscoelastic wave propagation simulations using the staggered-grid finite-difference code Anelastic Wave Propagation (AWP)-ODC (Olsen, 1994; Cui *et al.*, 2010, 2013) (with suffix derived from the authors Olsen, Day, and Cui). AWP-ODC has support for surface topography via a curvilinear transformation (O'Reilly *et al.*, 2021) where we used the digital elevation model from the 3D elevation program (U.S. Geological Survey, 2020) with a resolution of 30 m. See Text S2 for more details about the numerical simulations.

We tested eight different models for the ShakeOut scenario with increasing complexity, incrementally incorporating refinements into CVMS and the SSAF models that have emerged since the 2008 study (see Table 1). Our reference model number 1 consists of CVMS and SSAF from the CFM (CFM3, see Data and Resources for more details) used in the ShakeOut simulations by Graves *et al.* (2008, 2011), Olsen *et al.* (2009), Bielak *et al.* (2010), and Fuis *et al.* (2017). CVMS is then replaced by the more recent CVMSI in model number 2, used as the reference model for all the following models. Note that CVMS contains nearly homogeneous velocity structure outside the major basins (i.e., Los Angeles, San Fernando, San Gabriel, Chino, and San Bernardino basins) and the immediate surroundings (Fig. 2a), whereas CVMSI reveals substantially higher spatial complexity (Fig. 2b).

Surface topography is flat in model numbers 1 and 2 to capture the ground-motion response from the early ShakeOut simulations but is included in model numbers 3–8. Models numbered 4 and 5 incorporate the high-resolution 3D V_P models from travel-time tomography for the Imperial (Persaud *et al.*, 2016) and Coachella (Ajala *et al.*, 2019) valleys and the V_S model for the San Gabriel, Chino, and San Bernardino basins from ambient noise tomography (Li *et al.*, 2023) into CVMSI. The empirical relations by Brocher (2005) are used to derive density, as well as V_P or V_S if not available in the high-resolution models. We use the windowing approach by Ajala and Persaud (2021) to ensure smooth transitions between the high-resolution models and CVMSI (see Text S1 for more details). Figure 2c shows that the addition of the local models further increases the spatial resolution of the model around the SSAF as well as in the basins.

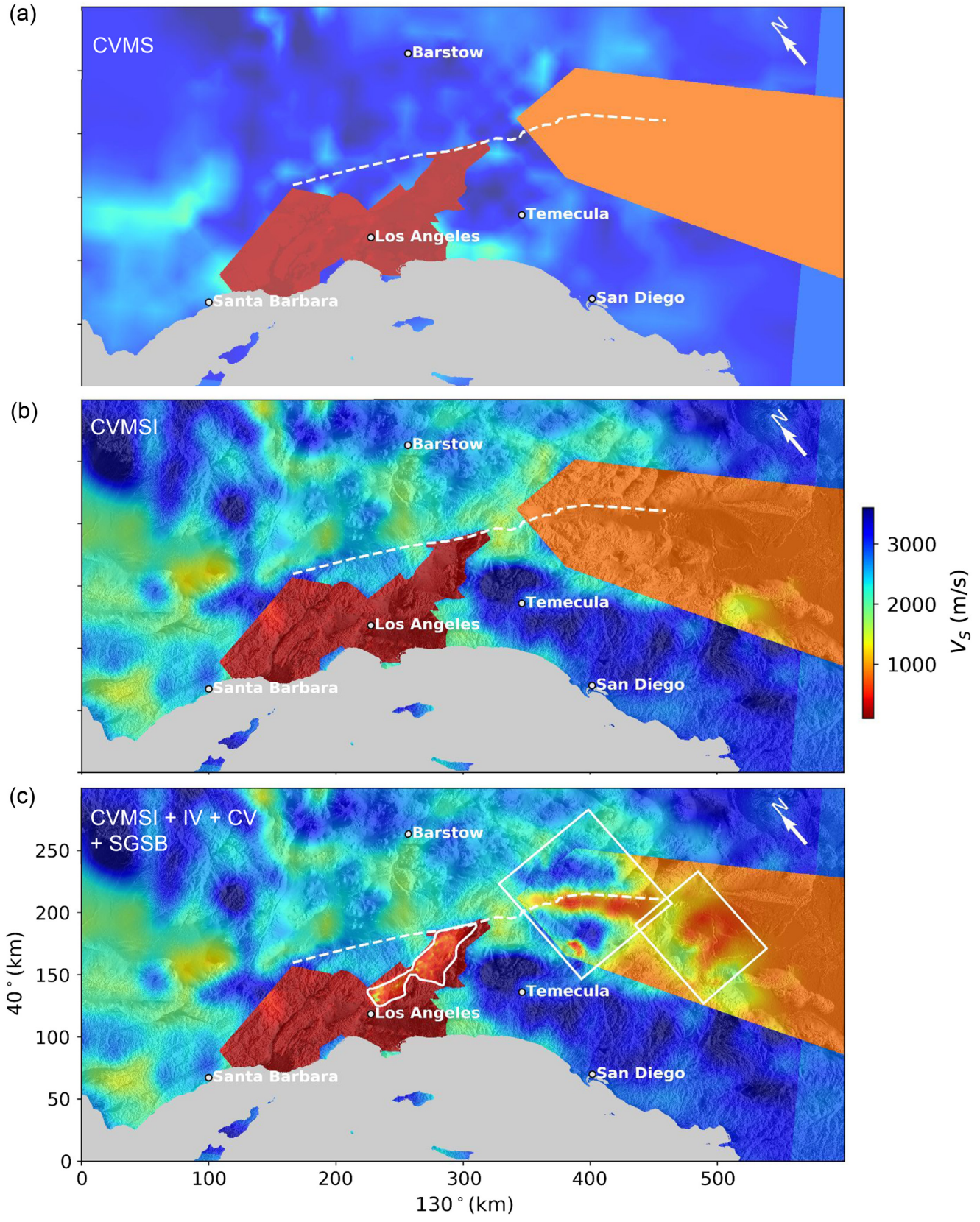

Figure 2. V_S at the free surface within the simulation domain for (a) Community Velocity Model version S4 (CVMS), (b) CVM-S4.26.M01 (CVMSI), and (c) CVMSI with local high-resolution models incorporated, with the fault trace depicted by a dashed curve. (c) The white polygons correspond to the domains of the local high-resolution models outlined in Figure 1. The color version of this figure is available only in the electronic edition.

Model number 6 introduces a near-surface low-velocity taper (LVT) using the approach of Ely *et al.* (2010), which has been shown to alleviate significant underprediction at sites outside the major basins where seismic speeds at shallow depths (top ~1 km) are unrealistically high in CVMSI (Hu *et al.*, 2022b). The LVT is constrained by its depth extent (here 700 m, defined as the tapering depth, z_T) and the local V_{S30} information (Thompson, 2018). See Text S3 for additional details on the implementation of the LVT. Model number 7 includes a more accurate subsurface fault geometry (also see Text S1) derived from the Salton Seismic Imaging Project by Fuis *et al.* (2017). Finally, in model number 8, we superimposed a statistical distribution of velocity and density heterogeneities (SSH) by Lin and Jordan (2023) to include the effects of unresolved velocity structure at shorter wavelengths (Text S4 provides additional details).

In all our simulations, we assumed that the quality factor is frequency independent and proportional to local S wavespeeds (V_S) (Olsen *et al.*, 2003), namely $Q_S = 0.1\ V_S$ and $Q_P = 2Q_S$. This attenuation model has been found to be the optimal for southern California by Hu *et al.* (2022a,b) and Yeh and Olsen (2023), whereas it differs from the attenuation model of $Q_S = 0.05\ V_S$ used in previous ShakeOut simulations (Graves *et al.*, 2008, 2011; Olsen *et al.*, 2009; Bielak *et al.*, 2010; Fuis *et al.*, 2017).

Simulation Results

Because of the long-period nature of the waveguide amplification and to allow comparison with the results documented in the early ShakeOut studies, the simulations here are primarily presented in terms of horizontal spectral acceleration at a period of 3 s (3 s-SA) with 5% damping following Boore (2010). PGVs of the corresponding models are provided in Figure S4.

Model number 1 reproduces the general features as found in the early ShakeOut studies (Graves *et al.*, 2008, 2011; Olsen *et al.*, 2009; Bielak *et al.*, 2010) in particular the strong long-period waveguide channeling of waves from the San Gabriel into the Los Angeles basin, as well as another southern branch of the waveguide entering the Los Angeles basin from the southeast (near Yorba Linda, see Fig. 3a). Replacing CVMS with CVMSI reduces 3 s-SA values by up to 65%–100% along both branches of the waveguide (compare Fig. 3a,b, and see Fig. S5 for percent difference), with PGVs reduced by 61% and 94% on east–west (E–W) and north–south (N–S) components, respectively, at station RUS, which is located within the northern branch of the waveguide (Fig. 4b). In contrast, the 3 s-SA values are increased by 20% in the mountainous areas just north of the San Gabriel and San Bernardino basins for CVMSI (30%–50% increase for PGV, see Fig. S5). Surface topography further reduces the 3 s-SA values in the Los Angeles basin by ~30%, in particular along the southern branch of the waveguide (Fig. 3c, Fig. S6). However, surface topography does not always reduce the long-period ground motions; specifically outside the basins, surface topography can increase the 3 s-SA by up to 35%–55% (e.g., between Rowland Heights and Covina, as well as the San Gabriel Mountains, see also Fig. S6).

Including the high-resolution tomography models for the Imperial (Persaud *et al.*, 2016) and Coachella (Ajala *et al.*, 2019) valleys into the CVMSI (model number 4) increases 3 s-SA values by 30%–50% at distances of 20 km northwest along the southern branch of the waveguide (Fig. 3d, Fig. S7). The addition of the northern high-resolution basin model (San Gabriel–Chino–San Bernardino basins [SGSB]) (Li *et al.*, 2023) in model number 5 increases 3 s-SA by 40%–100% for the northern half of the Chino and San Bernardino basins, as well as part of the San Gabriel and Los Angeles basins (Fig. 3e, Fig. S8). The primary influence of the SGSB model is confined to the San Bernardino, Chino, and the San Gabriel basins within the SGSB model domain, as well as the Los Angeles basin which is outside the domain (Fig. S8).

Figure 3f shows the effect of including an LVT in the CVMSI with the local high-resolution models and topography (model number 6) in the ShakeOut scenario simulations. The LVT increases the 3 s-SA values by 60%–80% in the near-fault areas along the SSAF where wavespeeds at shallow depths (0–1 km) in CVMSI are unrealistically high (Fig. 3f, Fig. S9), whereas the strongest waveguide amplification is reduced from the reduction in velocity contrast to the surrounding rock (e.g., southwest of the San Gabriel valley). The updated subsurface fault geometry from Fuis *et al.* (2017) in model number 7 reduces the near-fault 3 s-SA values on the western side of the SSAF in the near-fault areas but increases the 3 s-SA values in the San Gabriel Mountains, likely due to the change of radiation pattern associated with the updated dip angle of the fault (see Fig. 3g, Fig. S10). Finally, model number 8 (Fig. 3h) shows average 3 s-SA values for an ensemble of five realizations with the statistical distribution of heterogeneities obtained by Lin and Jordan (2023) on top of model number 7 (see in Figs. S11 and S12 for the variation among individual realizations). The presence of the statistical distribution of heterogeneities promotes seismic scattering leading to weaker 3 s-SA on average, particularly evident in the basins (20%–30% reduction within the Chino and San Bernardino basins, as well as in the Los Angeles basin, see Fig. 3h, Fig. S13).

Figure 4 shows 0–1 Hz synthetic waveforms for model numbers 1, 2, 3, and 8 (with one of the five realizations including the statistical model by Lin and Jordan, 2023), illustrating the dramatic reduction of velocity amplitudes in the waveguide (see station RUS) as model features are added or revised. Similar reduction can be found at station CLT, located 10 km from the fault near the eastern edge of the San Bernardino basin. On the other hand, the stations USC (downtown Los Angeles) and DLA (near the deepest portion of the Los Angeles basin) experience only slight reduction in the long-period peak velocities in the model with all added or revised model features. Figure S14 illustrates the combined contribution of all the model modifications applied to the reference

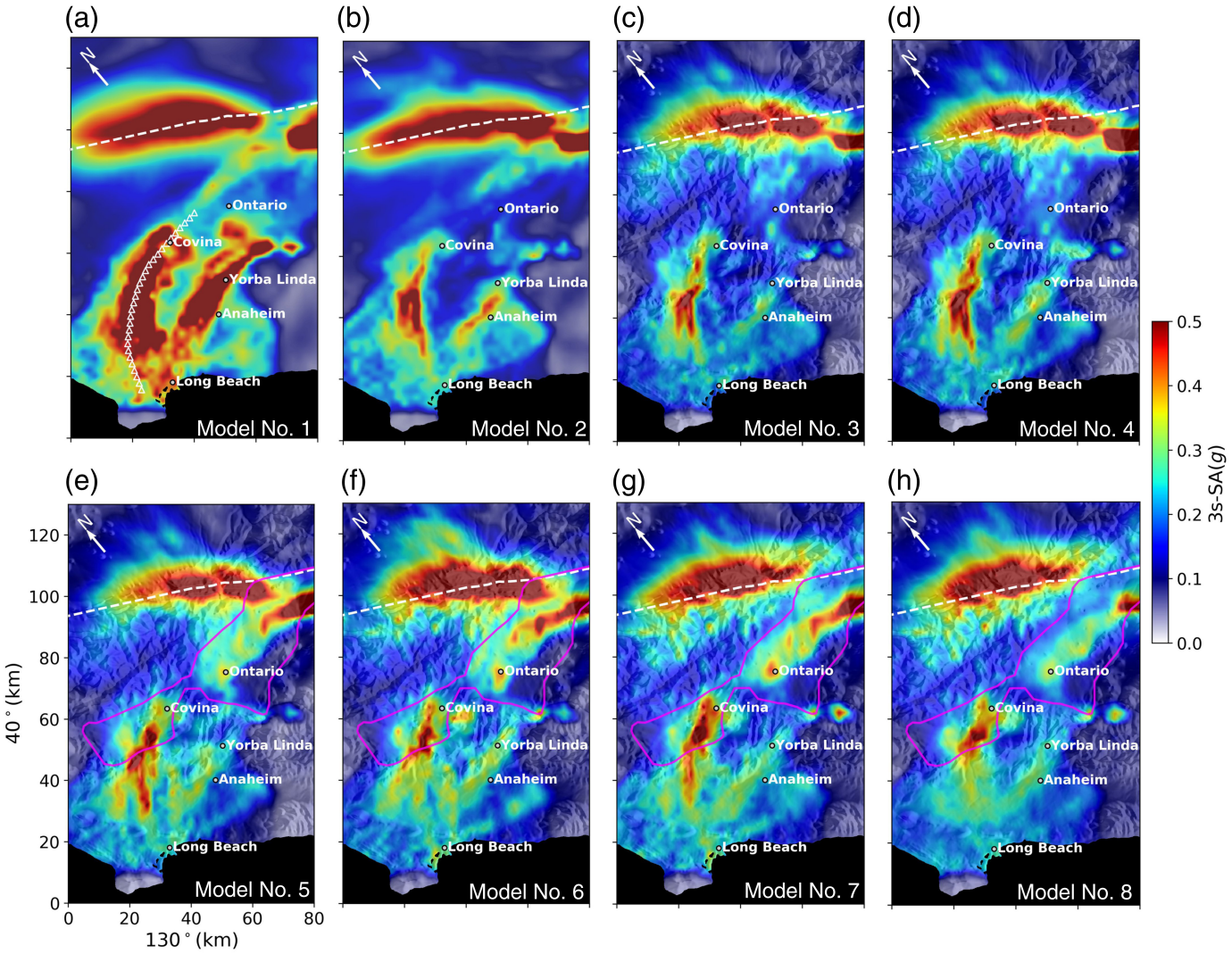

model (CVMS, model number 1) on the 3 s-SA and long-period PGVs. Both ground-motion measures are greatly reduced in most of the basin areas, and particularly along both branches of the waveguide (more than 60% decrease), and significantly increased in the San Gabriel Mountains (60%–100% for 3 s-SA and 100%–250% PGV).

Discussion and Conclusions

We have simulated 0–1 Hz physics-based ground motions for the **M** 7.8 ShakeOut scenario with eight different models (Table 1), illustrating the evolution in complexity since the first results in 2008. The most substantial changes in long-period ground motions, primarily reduction in the basin areas, occur when the CVMS model is updated to CVMSI (Lee *et al.*, 2014), which provides much improved resolution outside the major basins. Snapshots of surface velocity synthetics (Fig. S15) confirm that the weakened ground motions in the major basins are caused by increased seismic scattering of surface waves from increased spatial complexity prior to entering the basins in CVMSI (Fig. 2b), as compared to CVMS (Fig. 2a). The introduction of surface topography further increases the seismic scattering and reduces the coherence of the surface waves before they enter the basins (see snapshots in Fig. S16).

Figure 3. Spectral acceleration at a period of 3 s (3 s-SA) distributions in the greater Los Angeles area (see Fig. 1 for location of inset) for the eight models listed in Table 1. (a–h) Model number is labeled at lower right corner in each panel. The magenta polygon outlines the domain of the SGSB model (Li *et al.*, 2023) when included. The dashed line depicts the surface projection of the SSAF that ruptured in the ShakeOut scenario. (a) The triangles are the locations of the virtual array along the axis of the waveguide for comparison of simulations and ground-motion models (GMMs). The results for model number 8 shows the average over the five realizations with the statistical model by Lin and Jordan (2023) included. The color version of this figure is available only in the electronic edition.

Incorporating local high-resolution models into the CVMSI changes the long-period ground-motion pattern in different ways. The addition of the Imperial and Coachella valley models (Ajala *et al.*, 2019) leads to higher ground motions in the Los Angeles basin along the southern branch of the waveguide, whereas the SGSB model increases 3 s-SA values by up to

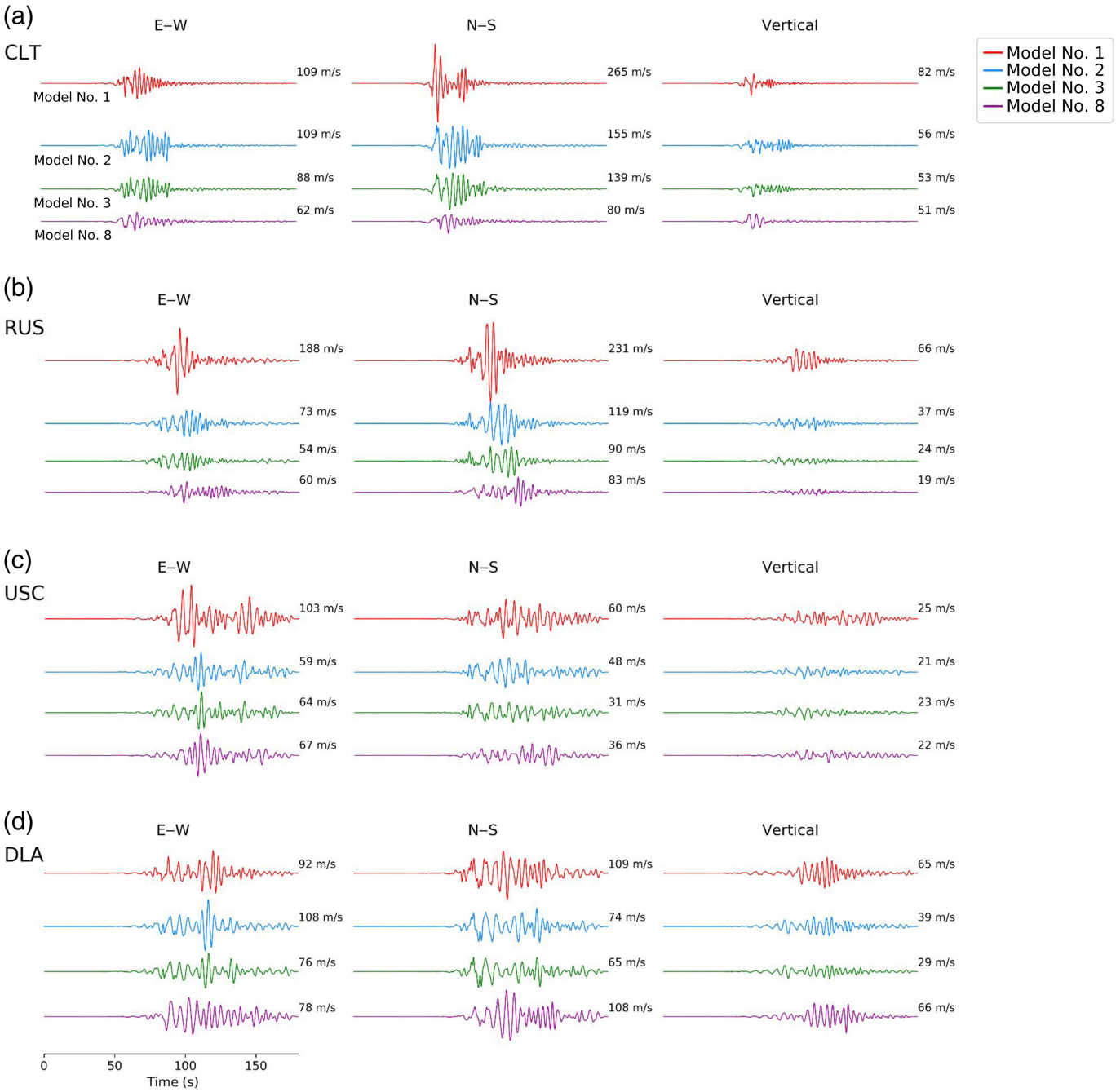

Figure 4. Comparison of synthetic waveforms for the ShakeOut scenario at select stations. (a) CLT (San Bernardino), (b) RUS (Whittier Narrows), (c) USC (Downtown Los Angeles), and (d) DLA (Cerritos) (see inset map in Fig. 1 for locations), for model numbers 1, 2, 3, and 8. The results for model number 8 are from one of the five realizations with the statistical model by Lin and Jordan (2023) included. See Table 1 for more details. The peak velocity is listed to the right of each trace. The color version of this figure is available only in the electronic edition.

80%–120% in the San Bernardino and Chino basins due to slower and deeper basin structures. Our results suggest that the velocity structure both inside and outside the basins substantially impact the long-period waves propagating in greater Los Angeles during a large earthquake on the SSAF.

The ultimate test of the strength of channeling of waves through a waveguide into the Los Angeles basin must await seismic recordings from a future large, northwestward-propagating rupture on the SSAF. However, until then, some confidence in the updated ShakeOut simulation results can be gained using seismic data from smaller earthquakes in the model region. For example, Taborda *et al.* (2016) obtained an improved fit to seismic records from simulations of 30 small earthquakes with our model number 2 (including the full-waveform tomographic improvements by Lee *et al.* (2014) as compared to model number 1 used in the early ShakeOut simulations. To test the effect of the combination of all the added features considered in our study, Figure 5

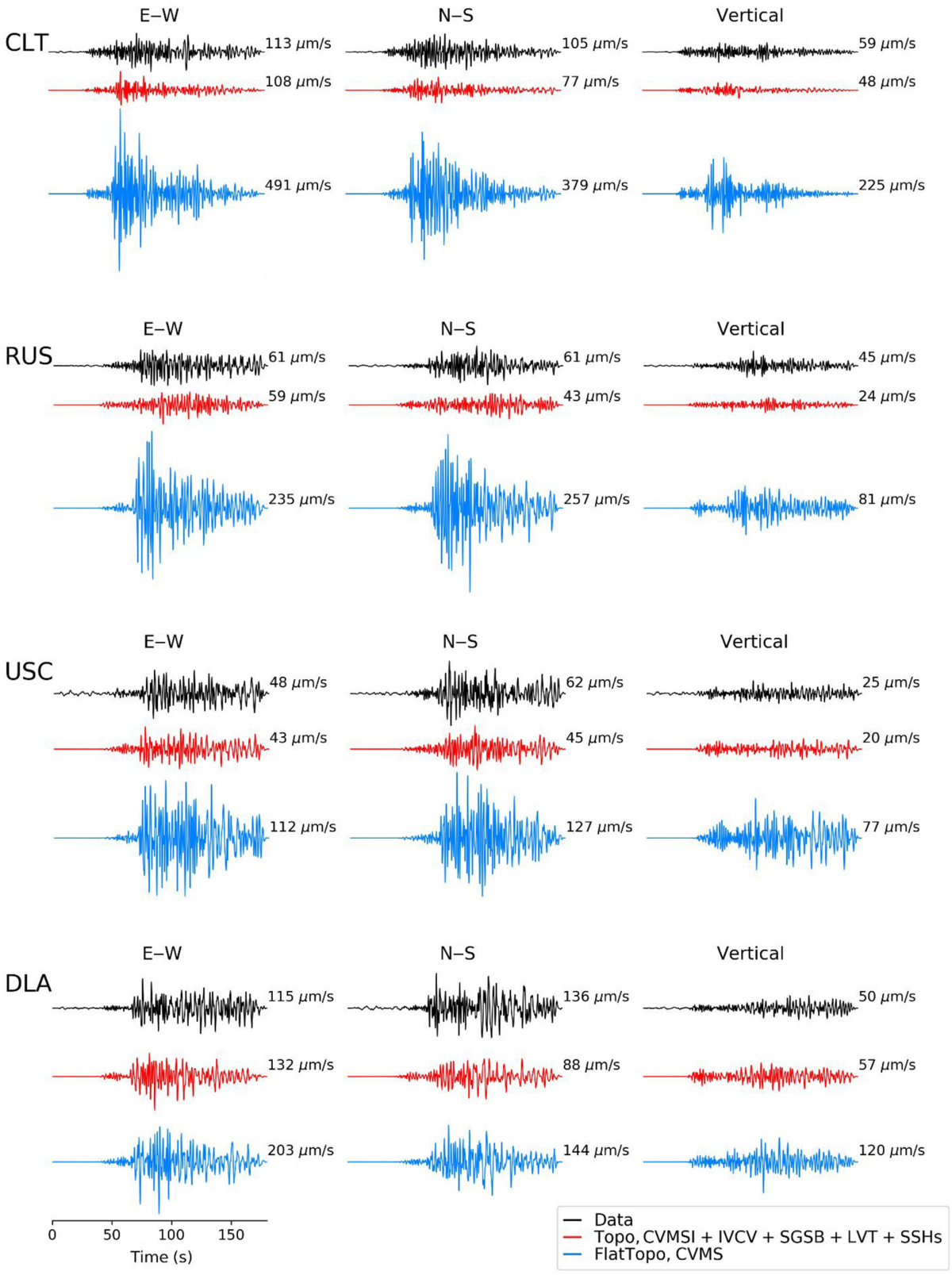

Figure 5. Comparison of (black) observed and synthetic waveforms for the 2016 **M** 4.3 event at stations (a) CLT, (b) RUS, (c) USC, and (d) DLA (see inset map in Fig. 1 for locations). Synthetics in blue and red are derived using model numbers 1 and 8, respectively (see Table 1). The peak velocities are listed to the right of each trace. The color version of this figure is available only in the electronic edition.

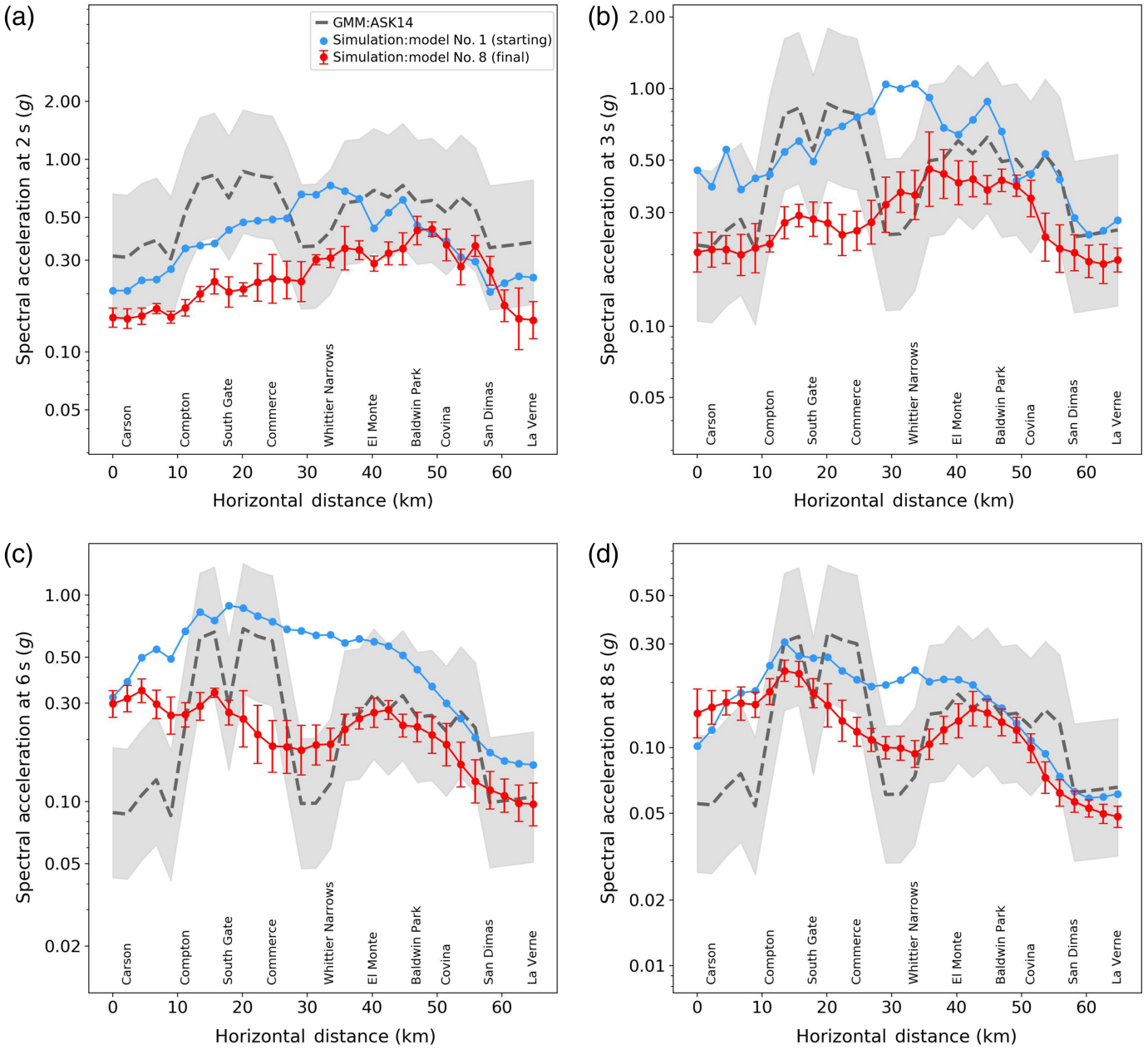

compares synthetics from model numbers 1 and 8 to recorded data at stations RUS, USC, DLA, and CLT for a 2016 **M** 4.3 event (see Data and Resources). The epicenter of this event, at Bombay Beach on the eastern edge of the Salton Sea (see red star in Fig. 1) coincides with that of the ShakeOut scenario, radiating part of its energy along the SAF corridor toward the waveguide into the Los Angeles basin. The large overprediction of the seismic data using model number 1 as well as the much improved fit obtained from the simulation using model number 8 for the **M** 4.3 event support our conclusions for the ShakeOut scenario.

Figure 6 shows spectral accelerations at periods of 2, 3, 6, and 8 s along a virtual array consisting of 30 stations along the axis of the northern branch of the waveguide, starting from Carson on the southwestern end to La Verne on the northeastern end (triangles in Fig. 3a) for the starting model (number 1) and the final model (number 8). Note the large decrease in spectral accelerations from model numbers 1 to 8, such as 60%, 65%, 70%, and 60% at periods of 2, 3, 6, and 8 s, respectively, at

Figure 6. Comparison of simulated spectral accelerations at periods of (a) 2 s, (b) 3 s, (c) 6 s, and (d) 8 s along the virtual array in Figure 3a for model numbers 1 and 8. The final model (number 8) depicts the mean and standard deviation of the values from five realizations with the statistical model by Lin and Jordan (2023). The median values predicted by the Next Generation Attenuation (NGA)-West2 GMM ASK14 (Abrahamson *et al.*, 2014) is depicted by the dashed line, and the gray shading indicates one standard deviation range. The color version of this figure is available only in the electronic edition.

Whittier Narrows and consistently west of Baldwin Park at periods of 2, 3, and 6 s. Figure 6 also compares 2 s-SA, 3 s-SA, 6 s-SA, and 8 s-SA values from our simulations to the Next Generation Attenuation (NGA)-West2 (Bozorgnia *et al.*, 2014) ground-motion model (GMM) ASK14 (Abrahamson *et al.*, 2014) for the ShakeOut scenario results using model numbers 1 and 8. In general, our simulated values along the virtual array for model number 8 match the median predictions by ASK14 within one standard deviation.

On the other hand, other NGA-West 2 GMMs, such as BSSA14 (Boore *et al.*, 2014), CB14 (Campbell and Bozorgnia, 2014), and CY14 (Chiou and Youngs, 2014), tend to predict much lower spectral accelerations inside the waveguide, except for the eastern end of the array in La Verne (see Text S5 and Figs. S17–S19 for details). This finding is consistent with Filippitzis *et al.* (2021) in which predictions from GMMs were compared to strong motion recordings for the 2019 **M** 7.1 Ridgecrest earthquake, lending some credibility to ASK14 for large events in southern California. The predictions from the four different GMMs tend to vary substantially depending on period (Figs. S17–S19). Such large uncertainties in the GMMs are likely caused by lack of data for larger events as well as differences in their corrections for basin response (e.g., in terms of Z1.0, depth to $V_S = 1000$ m/s) and local site response using V_{S30}. However, the basin amplification correction for ASK14 appears to be too large between Compton and Whittier Narrows, near the deepest section of Los Angeles basin (Fig. 6). This result suggests that physics-based simulations may help improve the accuracy of basin response in GMMs in future studies.

Additional factors to those analyzed in this study may affect the long-period ground motions for a large earthquake on the SSAF. Spontaneous rupture simulations with a dynamic version of the ShakeOut scenario source using the slip-matching technique (Dalguer *et al.*, 2008; Olsen *et al.*, 2009) revealed significant reduction in wavefield coherency and long-period (3 s-SA) spectral accelerations compared to the ShakeOut scenario for the kinematic source description (Olsen *et al.*, 2009). In addition, Roten *et al.* (2014, 2016, 2023) showed that nonlinear effects can reduce large long-period surface-wave ground motions along the waveguides in greater Los Angeles. The weakened surface waves entering the basin, however, are likely to result in much less nonlinear damping within the major basins than originally anticipated in Roten *et al.* (2023), which used the older CVMS. We recommend that future simulation studies test whether refinement of the source description or including nonlinear damping can further affect the long-period ground motions from the ShakeOut scenario.

Seismic anelastic attenuation is another factor impacting the predicted ground-motion levels for the ShakeOut scenario. Here, we assume the *S*-wave quality factor to be $Q_S = 0.1V_S$ (V_S in meters per second), which has been shown to generate optimal fit to data in southern California by recent ground-motion modeling studies (Hu *et al.*, 2022a; Yeh and Olsen, 2023). Hu *et al.* (2022a) furthermore showed that an attenuation model using a nonlinear relation between Q_S and V_S (such as the polynomial model used in Taborda and Bielak, 2014) does not significantly change the fit to data as compared to the simple linear Q_S–V_S relationship used here. Thus, uncertainty in the attenuation structure in southern California is unlikely to change our conclusions regarding the added and revised model features. However, we recommend that new area-specific information on the attenuation structure in southern California be incorporated into the ground-motion simulations when available, such as the recent attenuation tomography results by Nardoni and Persaud (2024) from ambient noise imaging.

In summary, our simulations suggest that long-period ground motions for the ShakeOut scenario in the densely populated Los Angeles area have been severely overestimated based on low-resolution velocity models and fault structure, as well as omission of model features such as surface topography. Our findings are in agreement with a recent study by Rood *et al.* (2024), showing that the mean hazard ground motion is overestimated by 65% along the SSAF using analysis of precariously balanced rocks. We recommend that the ground-motion predictions for the ShakeOut scenario be revisited using the result of our study to produce refined risk analysis for the greater Los Angeles area.

Data and Resources

The authors used the tool by Mongold and Baker (2021) to compute spectral accelerations from ground-motion models (GMMs), providing all available fault-related site-specific parameters, whenever applicable. The open-source numerical simulation code AWP-ODC can be freely accessed via github (https://github.com/SCECcode/awp, last accessed August 2023). The Statewide California Earthquake Center (SCEC) Unified Community Velocity Model (UCVM) tool can be accessed via github at https://github.com/SCECcode/UCVMC (last accessed August 2023). The velocity models of Imperial and Coachella valleys can be accessed through Patricia Persaud's personal website (https://www.geo.arizona.edu/~ppersaud/Data.html, last accessed October 2023). The SCEC Community Fault Model (CFM) mentioned in this study refers to CFM3 (Plesch *et al.*, 2007), which can be accessed via the SCEC CFM website (https://southern.scec.org/research/cfm, last accessed August 2023). Focal mechanism and location of the **M** 4.3 event (event ID ci37701544) used for validation were accessed from the U.S. Geological Survey (USGS) website (https://earthquake.usgs.gov/earthquakes/eventpage/ci37701544/executive, last accessed August 2024). The strong motion recordings of the **M** 4.3 event were downloaded using the data fetch tool distributed by Incorporated Research Institutions for Seismology (IRIS). The supplemental material provides additional details about the development of the velocity and source rupture models, figures illustrating the differences in ground motions between models, and a movie of the surface ground velocities simulated for the starting and the final models.

Declaration of Competing Interests

The authors acknowledge that there are no conflicts of interest recorded.

Acknowledgments

The authors thank Robert Graves for providing the kinematic source models used in this study via personal communication. The authors are also grateful to Patricia Persaud for providing access to velocity models of the Imperial and Coachella valleys (also available in the Statewide California Earthquake Center [SCEC] Unified Community Velocity Model [UCVM] software). The authors appreciate the constructive comments from Patricia Persaud and an anonymous reviewer that helped improve the article. This research used resources of the Oak Ridge Leadership Computing Facility at the Oak Ridge National Laboratory, which is supported by the Office of Science of the U.S. Department of Energy under Contract Number DE-AC05-00OR22725 and was supported through SCEC (Contribution Number 13577). SCEC is funded by National Science Foundation (NSF) Cooperative Agreement EAR-1600087 and U.S. Geological Survey (USGS) Cooperative Agreement G17AC00047.

References

Abrahamson, N. A., W. J. Silva, and R. Kamai (2014). Summary of the ASK14 ground motion relation for active crustal regions, *Earthq. Spectra* **30,** no. 3, 1025–1055, doi: 10.1193/070913EQS198M.

Ajala, R., and P. Persaud (2021). Effect of merging multiscale models on seismic wavefield predictions near the southern San Andreas fault, *J. Geophys. Res.* **126,** no. 10, e2021JB021915 , doi: 10.1029/2021JB021915.

Ajala, R., P. Persaud, and A. Juarez (2022). Earth model-space exploration in southern California: Influence of topography, geotechnical layer, and attenuation on wavefield accuracy, *Front. Earth Sci.* **10,** doi: 10.3389/feart.2022.964806.

Ajala, R., P. Persaud, J. M. Stock, G. S. Fuis, J. A. Hole, M. Goldman, and D. Scheirer (2019). Three-dimensional basin and fault structure from a detailed seismic velocity model of Coachella valley, southern California, *J. Geophys. Res.* **124,** no. 5, 4728–4750, doi: 10.1029/2018JB016260.

Bielak, J., R. W. Graves, K. B. Olsen, R. Taborda, L. Ramírez-Guzmán, S. M. Day, G. P. Ely, D. Roten, T. H. Jordan, P. J. Maechling, *et al.* (2010). The ShakeOut earthquake scenario: Verification of three simulation sets, *Geophys. J. Int.* **180,** no. 1, 375–404, doi: 10.1111/j.1365-246X.2009.04417.x.

Boore, D. M. (2010). Orientation-independent, nongeometric-mean measures of seismic intensity from two horizontal components of motion, *Bull. Seismol. Soc. Am.* **100,** no. 4, 1830–1835, doi: 10.1785/0120090400.

Boore, D. M., J. P. Stewart, E. Seyhan, and G. M. Atkinson (2014). NGA-West2 equations for predicting PGA, PGV, and 5% damped PSA for shallow crustal earthquakes, *Earthq. Spectra* **30,** no. 3, 1057–1085, doi: 10.1193/070113EQS184M.

Bozorgnia, Y., N. A. Abrahamson, L. A. Atik, T. D. Ancheta, G. M. Atkinson, J. W. Baker, A. Baltay, D. M. Boore, K. W. Campbell, B. S.-J. Chiou, *et al.* (2014). NGA-West2 research project, *Earthq. Spectra* **30,** no. 3, 973–987, doi: 10.1193/072113EQS209M.

Brocher, T. M. (2005). Empirical relations between elastic wavespeeds and density in the earth's crust, *Bull. Seismol. Soc. Am.* **95,** no. 6, 2081–2092, doi: 10.1785/0120050077.

Campbell, K. W., and Y. Bozorgnia (2014). NGA-West2 ground motion model for the average horizontal components of PGA, PGV, and 5% damped linear acceleration response spectra, *Earthq. Spectra* **30,** no. 3, 1087–1115, doi: 10.1193/062913EQS175M.

Chiou, B. S.-J., and R. R. Youngs (2014). Update of the Chiou and Youngs NGA model for the average horizontal component of peak ground motion and response spectra, *Earthq. Spectra.* **30,** no. 3, 1117–1153, doi: 10.1193/072813EQS219M.

Cui, Y., K. B. Olsen, T. H. Jordan, K. Lee, J. Zhou, P. Small, D. Roten, G. Ely, D. K. Panda, A. Chourasia, *et al.* (2010). Scalable earthquake simulation on petascale supercomputers, *SC'10: Proc. of the 2010 ACM/IEEE International Conf. for High Performance Computing, Networking, Storage and Analysis*, New Orleans, Los Angeles, 13–19 November 2010.

Cui, Y., E. Poyraz, K. B. Olsen, J. Zhou, K. Withers, S. Callaghan, J. Larkin, C. Guest, D. Choi, A. Chourasia, *et al.* (2013). Physics-based seismic hazard analysis on petascale heterogeneous supercomputers, *SC'13: Proc. of the International Conf. on High Performance Computing, Networking, Storage and Analysis*, Denver, Colorado, November 2013, 1–12.

Dalguer, L., S. Day, K. Olsen, and V. Cruz-Atienza (2008). Rupture models and ground motion for Shakeout and other southern San Andreas fault scenarios, *Proc. of 14th World Conf. on Earthquake Engineering*, Beijing, China, 12–17 October 2008.

Day, S. M., D. Roten, and K. B. Olsen (2012). Adjoint analysis of the source and path sensitivities of basin-guided waves, *Geophys. J. Int.* **189,** no. 2, 1103–1124, doi: 10.1111/j.1365-246X.2012.05416.x.

Ely, G. P., T. Jordan, P. Small, and P. J. Maechling (2010). A V_{S30}-derived nearsurface seismic velocity model, *Eos Trans. AGU* (Fall Meet. 2010), San Francisco, California, Abstract S51A-1907.

Field, E. H. (2008). The Uniform California Earthquake Rupture Forecast, version 2 (UCERF 2), *U.S. Geol. Surv. Open-File Rept. 2007-1437.*

Filippitzis, F., M. D. Kohler, T. H. Heaton, R. W. Graves, R. W. Clayton, R. G. Guy, J. J. Bunn, and K. M. Chandy (2021). Ground motions in urban Los Angeles from the 2019 Ridgecrest earthquake sequence, *Earthq. Spectra* **37,** no. 4, 2493–2522, doi: 10.1177/87552930211003916.

Fuis, G. S., K. Bauer, M. R. Goldman, T. Ryberg, V. E. Langenheim, D. S. Scheirer, M. J. Rymer, J. M. Stock, J. A. Hole, R. D. Catchings, *et al.* (2017). Subsurface geometry of the San Andreas fault in southern California: Results from the Salton Seismic Imaging Project (SSIP) and strong ground motion expectations, *Bull. Seismol. Soc. Am.* **107,** no. 4, 1642–1662, doi: 10.1785/0120160309.

Graves, R. W., B. T. Aagaard, and K. W. Hudnut (2011). The ShakeOut earthquake source and ground motion simulations, *Earthq. Spectra.* **27,** no. 2, 273–291, doi: 10.1193/1.3570677.

Graves, R. W., B. T. Aagaard, K. W. Hudnut, L. M. Star, J. P. Stewart, and T. H. Jordan (2008). Broadband simulations for M_w 7.8 southern San Andreas earthquakes: Ground motion sensitivity to rupture speed, *Geophys. Res. Lett.* **35,** no. 22, doi: 10.1029/2008GL035750.

Hu, Z., K. B. Olsen, and S. M. Day (2022a). 0-5 Hz deterministic 3-D ground motion simulations for the 2014 La Habra, California, earthquake, *Geophys. J. Int.* **230,** no. 3, 2162–2182, doi: 10.1093/gji/ggac174.

Hu, Z., K. B. Olsen, and S. M. Day (2022b). Calibration of the near-surface seismic structure in the SCEC community velocity model version 4, *Geophys. J. Int.* **230,** no. 3, 2183–2198, doi: 10.1093/gji/ggac175.

Jones, L. M., and M. Benthien (2011). Preparing for a "Big One": The Great Southern California ShakeOut, *Earthq. Spectra.* **27,** no. 2, 575–595, doi: 10.1193/1.3586819.

Jones, L. M., R. L. Bernknopf, D. A. Cox, J. Goltz, K. W. Hudnut, D. S. Mileti, S. Perry, D. Ponti, K. A. Porter, M. S. Reichle, *et al.* (2008). *The ShakeOut Scenario: Effects of a Potential M 7.8 Earthquake on the San Andreas Fault in Southern California*, U.S. Geological Survey, Reston, Virginia.

Kohler, M. D., H. Magistrale, and R. W. Clayton (2003). Mantle heterogeneities and the SCEC reference three-dimensional seismic velocity model version 3, *Bull. Seismol. Soc. Am.* **93,** no. 2, 757–774, doi: 10.1785/0120020017.

Krishnan, S., and M. Muto (2008). *The ShakeOut Scenario Supplemental Study: High-Rise Steel Buildings*, SPA Risk LLC, Denver, Colorado.

Lee, E.-J., P. Chen, T. H. Jordan, P. B. Maechling, M. A. M. Denolle, and G. C. Beroza (2014). Full-3-D tomography for crustal structure in southern California based on the scattering-integral and the adjoint-wavefield methods, *J. Geophys. Res.* **119,** no. 8, 6421–6451, 10.1002/2014JB011346.

Li, Y., V. Villa, R. W. Clayton, and P. Persaud (2023). Shear wave velocities in the San Gabriel and San Bernardino basins, California, *J. Geophys. Res.* **128,** no. 7, e2023JB026488 , doi: 10.1029/2023JB026488.

Lin, Y.-P., and T. H. Jordan (2023). Elastic scattering dominates high-frequency seismic attenuation in southern California, *Earth Planet Sci. Lett.* **616,** 118227 , 10.1016/j.epsl.2023.118227.

Lynch, K. P., K. L. Rowe, and A. B. Liel (2011). Seismic performance of reinforced concrete frame buildings in southern California, *Earthq. Spectra* **27,** no. 2, 399–418, doi: 10.1193/1.3570684.

Magistrale, H., S. Day, R. W. Clayton, and R. Graves (2000). The SCEC Southern California reference three-dimensional seismic velocity model version 2, *Bull. Seismol. Soc. Am.* **90,** no. 6B, S65–S76, doi: 10.1785/0120000510.

Mongold, E., and J. Baker (2021). A software repository of ground motion models—Version 1.0.0., *Technical Rept. no. 207, Blume Earthquake Engineering Center*, Stanford Digital Repository, available at https://purl.stanford.edu/qy113my5899 (last accessed January 2024).

Nardoni, C., and P. Persaud (2024). Evidence for faulting and fluid-driven earthquake processes from seismic attenuation variations beneath metropolitan Los Angeles, *Sci. Rep.* **14,** no. 1, 17595 , doi: 10.1038/s41598-024-67872-3.

Olsen, K. B. (1994). Simulation of three-dimensional wave propagation in the Salt Lake basin, *Ph.D. Thesis*, University of Utah, Salt Lake City, Utah, 157 pp.

Olsen, K. B., S. M. Day, and C. R. Bradley (2003). Estimation of *Q* for long-period (>2 sec) waves in the Los Angeles basin, *Bull. Seismol. Soc. Am.* **93,** no. 2, 627–638, doi: 10.1785/0120020135.

Olsen, K. B., S. M. Day, L. A. Dalguer, J. Mayhew, Y. Cui, J. Zhu, V. M. Cruz-Atienza, D. Roten, P. Maechling, T. H. Jordan, *et al.* (2009). ShakeOut-D: Ground motion estimates using an ensemble of large earthquakes on the southern San Andreas fault with spontaneous rupture propagation, *Geophys. Res. Lett.* **36,** no. 4, doi: 10.1029/2008GL036832.

O'Reilly, O., T. Yeh, K. B. Olsen, Z. Hu, A. Breuer, D. Roten, and C. A. Goulet (2021). A High-order finite-difference method on staggered curvilinear grids for seismic wave propagation applications with topography, *Bull. Seismol. Soc. Am.* **112,** no. 1, 3–22, doi: 10.1785/0120210096.

Persaud, P., Y. Ma, J. M. Stock, J. A. Hole, G. S. Fuis, and L. Han (2016). Fault zone characteristics and basin complexity in the southern Salton trough, California, *Geology* **44,** no. 9, 747–750, doi: 10.1130/G38033.1.

Plesch, A., J. H. Shaw, C. Benson, W. A. Bryant, S. Carena, M. Cooke, J. Dolan, G. Fuis, E. Gath, L. Grant, *et al.* (2007). Community Fault Model (CFM) for southern California, *Bull. Seismol. Soc. Am.* **97,** no. 6, 1793–1802, doi: 10.1785/0120050211.

Porter, K., L. Jones, D. Cox, J. Goltz, K. Hudnut, D. Mileti, S. Perry, D. Ponti, M. Reichle, A. Z. Rose, *et al.* (2011). The ShakeOut scenario: A hypothetical M_w 7.8 earthquake on the southern San Andreas fault, *Earthq. Spectra* **27,** no. 2, 239–261, doi: 10.1193/1.3563624.

Rood, A. H., P. J. Stafford, and D. H. Rood (2024). San Andreas fault earthquake hazard model validation using probabilistic analysis of precariously balanced rocks and Bayesian updating, *Seismol. Res. Lett.* **95,** no. 3, 1776–1793, doi: 10.1785/0220220287.

Roten, D., Y. Cui, K. B. Olsen, S. M. Day, K. Withers, W. H. Savran, P. Wang, and D. Mu (2016). High-frequency nonlinear earthquake simulations on petascale heterogeneous supercomputers, *SC '16: Proc. of the International Conf. for High Performance Computing, Networking, Storage and Analysis*, Salt Lake City, Utah, 13–18 November 2016, 957–968.

Roten, D., K. B. Olsen, S. M. Day, Y. Cui, and D. Fäh (2014). Expected seismic shaking in Los Angeles reduced by San Andreas fault zone plasticity, *Geophys. Res. Lett.* **41,** no. 8, 2769–2777, doi: 10.1002/2014GL059411.

Roten, D., T. Yeh, K. B. Olsen, S. M. Day, and Y. Cui (2023). Implementation of Iwan-type nonlinear rheology in a 3D high-order staggered-grid finite-difference method, *Bull. Seismol. Soc. Am.* **113,** no. 6, 2275–2291, doi: 10.1785/0120230011.

Taborda, R., and J. Bielak (2014). Ground-motion simulation and validation of the 2008 Chino Hills, California, earthquake using different velocity models, *Bull. Seismol. Soc. Am.* **104,** no. 4, 1876–1898, doi: 10.1785/0120130266.

Taborda, R., S. Azizzadeh-Roodpish, N. Khoshnevis, and K. Cheng (2016). Evaluation of the southern California seismic velocity models through simulation of recorded events, *Geophys. J. Int.* **205,** no. 3, 1342–1364, doi: 10.1093/gji/ggw085.

Taciroglu, E., and P. Khalili-Tehrani (2008). *The ShakeOut Scenario Supplemental Study: Older Reinforced Concrete Buildings*, SPA Risk LLC, Denver, Colorado.

Thompson, E. M. (2018). An updated V_{S30} map for California with geologic and topographic constraints, *U.S. Geol. Surv. Data Release*, doi: 10.5066/F7JQ108S.

U.S. Geological Survey (2020). 3D elevation program 1-meter resolution digital elevation model, available at https://www.usgs.gov/3delevation-program (last accessed August 2023).

Yeh, T., and K. B. Olsen (2023). Fault damage zone effects on ground motions during the 2019 M_w 7.1 Ridgecrest, California, earthquake, *Bull. Seismol. Soc. Am.* **113,** no. 4, 1724–1738, doi: 10.1785/0120220249.

Manuscript received 7 June 2024
Published online 20 September 2024